CHARA TECHNICAL REPORT

NO. 24 27 NOVEMBER 1995

Correlation measurement and group delay tracking with a noisy detector

THEO TEN BRUMMELAAR

ABSTRACT: The use of a noisy detector for group delay tracking and/or correlation measurement in optical stellar interferometry is analyzed. Expressions are derived for the signal-to-noise ratio of correlation measurement and the probability of tracking loss in the presence of detector noise. It is shown that such a detector can be suitable for either measurement. For example, the high quantum efficiency of modern CCDs can offset the readout noise to a large extent, making them a good candidate for use in fringe tracking.

1. INTRODUCTION

When choosing a detector for optical stellar interferometry, many often conflicting requirements come into play, for example: detector quantum efficiency (DQE), noise, number of pixels, and cost. Ideally, a high DQE, low or even zero noise, multipixel detector is required, and all this at a reasonable cost. A popular detector for interferometry is the avalanche photo diode, or APD (Nightingale 1991), which is photon noise limited and, compared to photomultipliers and image intensifiers, has a high DQE. Unfortunately for many tasks, such as group delay tracking (GDT) or multiple band correlation measurement, large numbers of pixels are required. APD's are single pixel devices, and the financial and logistical cost of using them for multiband observation can be high. Photon noise limited array detectors are available — for example, the PAPA camera (Papaliolios & Mertz 1982) — although their DQE to date has been rather poor (Lawson 1993). Cameras based on charge coupled devices (CCD) are now being made with extremely high DQE and relatively low readout noise (Beletic et al. 1991). The question that then arises is: does the high DQE of the CCD compensate for the addition of readout noise?

There have been many studies of the effects of photon noise in optical stellar interferometry on fringe correlation measurement (Tango & Twiss 1980, Roddier 1986, Buscher 1988, Kulkarni et al. 1991, Beletic & Goody 1992) and group delay tracking (Lawson 1994, Beletic 1994). Except for the work done by Beletic (1994) for the Center for High Angular Resolution Astronomy (CHARA) Array (McAlister et al. 1994), all of these works assume a photon noise limited detector and ignore the effects of detector noise.

In the analysis that follows, equations are derived for the signal-to-noise (SNR) ratio of correlation measurement as well as for the probability of tracking loss using group delay

[1]Center for High Angular Resolution Astronomy, Georgia State University, Atlanta GA 30303-3083
Tel: (404) 651-2932, FAX: (404) 651-1389, Anonymous ftp: chara.gsu.edu, WWW: http://www.chara.gsu.edu

tracking in the presence of detector noise. Using these expressions, it is demonstrated that it is possible to measure fringe correlation and perform group delay tracking with a noisy detector as long as its DQE is high. In the case of group delay tracking, a CCD would be an excellent choice for a detector. In the case of correlation measurement it is shown that a CCD could be used but may not be the detector of choice. The decision will then come down to logistics and cost considerations. For example, if one already has invested in a highly efficient but noisy detector for fringe tracking, why not also use it for correlation measurement even though it may not be ideal for this application?

2. FRINGE AND DETECTOR MODEL

We will consider a two-beam setup for both the case of correlation measurement and that of fringe tracking. The extension to multiple beams then follows relatively easily. When combining two beams, one has the choice of using either the pupil or the image plane. From the point of view of photon noise, Roddier (1986) claims that the pupil plane provides better results whereas Buscher (1988) claims they are equivalent. We shall not specify which plane will be used but will consider two tilt corrected beams combined and imaged through a dispersive element onto a detector. These beams can either be combined in the pupil plane with measurements taken on either side of a beam splitter, or they can be combined in the image plane and viewed on a single array detector. The two methods are equivalent as far as the analysis to follow is concerned. For the sake of generality we assume that the fringes are measured on a 2-dimensional array detector where in one dimension the fringes are spread in phase and in the second dimension they are spread in wavelength. A temporal fringe encoding scheme, such as the one used in the Mark III interferometer (Shao et al. 1988) or that proposed by Tango & Twiss (1980), is equivalent to the phase dimension of an array detector. Alternatively a constant tilt could be introduced into one beam, or an image plane combination scheme could be used to introduce the phase spread on a detector. An example optical layout is given in Figure 1.

The two beams entering the system are assumed to have been tilt corrected and to have passed through an optical path length equalizer (OPLE) to arrive at the beam combiner with an optical path length difference (OPD) of x meters. Atmospheric effects beyond piston and tilt and residual aberrations due to the optical system will not be included in this analysis but are included in the coherence transfer factor η such that the measured visibility magnitude V is given by

$$V(\nu) = \eta\,|\gamma(\nu)| = \eta_{\rm s}\,\eta_{\rm t}\,\eta_{\rm o}\,|\gamma(\nu)| \tag{1}$$

where $\gamma(\nu)$ is the wavenumber ($\nu = 1/\lambda$) dependent visibility magnitude of the object at the current projected baseline. Expressions for the coherence transfer factor can be found for spatial effects of the atmosphere $\eta_{\rm s}$ in Tango & Twiss (1980) and temporal atmospheric effects $\eta_{\rm t}$ in Buscher (1988). The coherence transfer factor for the optical system itself $\eta_{\rm o}$, including any possible high order adaptive optics, can be approximated by the Strehl ratio for the system (ten Brummelaar et al. 1995).

The spread in phase across the first dimension of the detector will be written as

$$\Phi_i = \frac{2\pi i}{P_\Phi} s_\Phi \tag{2}$$

where i is the phase pixel number ranging from 1 to P_Φ and s_Φ is the spatial frequency of the fringes formed on the detector. In the example optical configuration given in Figure 1,

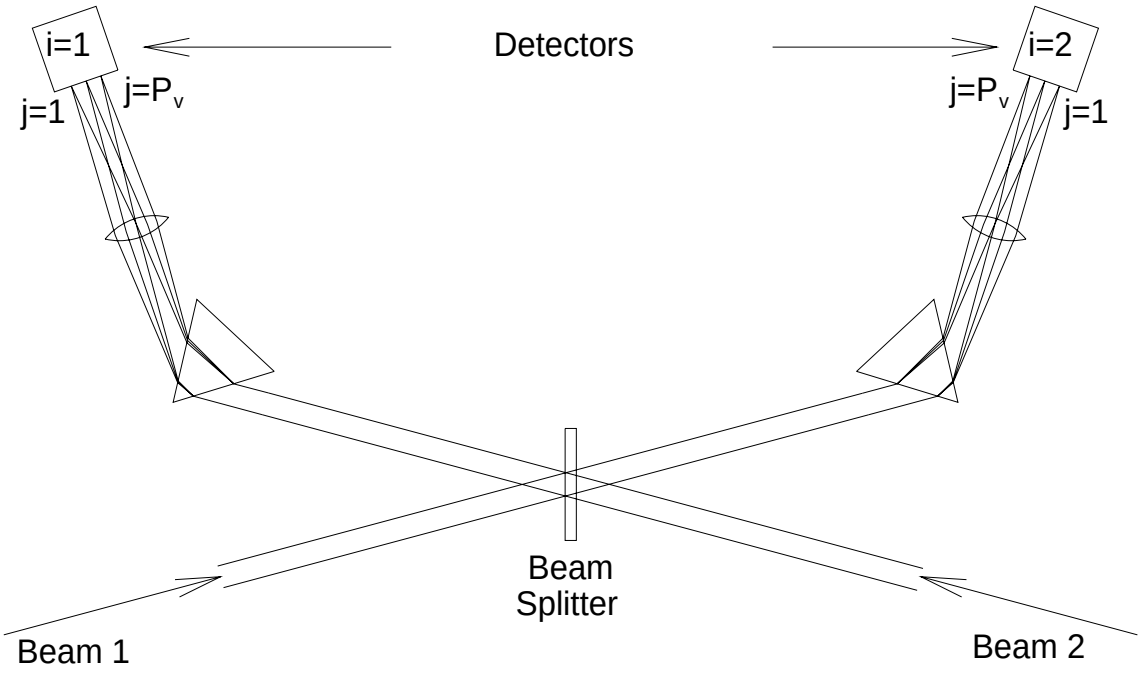

FIGURE 1. An optical layout for combining two beams. The two beams are combined in the pupil plane using a flat beam splitter. Each output beam is then fed through a dispersive element and imaged onto a detector.

there are only two sets of phase pixels, one on each of the detectors shown, with a phase difference of π radians. Thus in this case $P_\Phi = 2$ and $s_\Phi = 1$.

The pixels in the spectral dimension of the detector are arranged evenly in wavenumber ν. This can be done by rebinning the data collected by a detector linear in space, a process that can be performed noiselessly and on-chip in the case of a CCD or by software for a detector like the PAPA camera. Alternatively, one could use a dispersive optical system that directly produces a spectrum linear in space and wavenumber such as a grism (Traub 1990). If the pixels in each channel range from wavenumber ν_1 to wavenumber ν_{P_ν} the central wavenumber of the jth pixel is

$$\nu_j = \nu_1 + \frac{j}{P_\nu}(\nu_{P_\nu} - \nu_1) \tag{3}$$

where P_ν is the number of pixels across the spectrum. Each spectrum formed in this way will contain channel fringes with a spatial frequency directly related to the OPD $x(t)$ via

$$s_\nu(t) = x(t)(\nu_{P_\nu} - \nu_1) \tag{4}$$

which is the basis of group delay tracking to be discussed in Section 5.

We now write the light intensity measured in the ith phase pixel ($1 \le i \le P_\Phi$) and the jth

spectral pixel ($1 \leq j \leq P_\nu$) as

$$I_{ij}(t) = I_0 \times \left[1 + V(\nu_j) \cos \left(\underbrace{\frac{2\pi i}{P_\Phi} s_\Phi}_{\text{Phase Term}} + \underbrace{\frac{2\pi j}{P_\nu} s_\nu(t)}_{\text{Spectral Term}} + \underbrace{\Phi(t)}_{\text{Other Terms}} \right) \right] \tag{5}$$

where I_0 is the expected classical intensity from both apertures in a single pixel including the atmosphere and optical system performance and

$$\Phi(t) = 2\pi\nu_1 \, x(t) - \frac{2\pi s_\Phi}{P_\Phi} + \Phi_\gamma(\nu_j) + \Phi_{\text{atm}}(t). \tag{6}$$

The quantity $\Phi_\gamma(\nu_j)$ is the visibility phase, and $\Phi_{\text{atm}}(t)$ is the phase difference introduced by atmospheric turbulence. This intensity pattern is sampled by the detector at a sample time τ which will be of the order of the temporal coherence time of the atmosphere τ_0.

We are now in a position to write an expression for the expected number of counts measured in a given pixel during a single sample period. The count of photon events in phase pixel i and spectral pixel j during sample period k is written

$$n_{ijk} = c_{ijk} + r_{ijk} \tag{7}$$

where c_{ijk} is the signal term and r_{ijk} is the noise term. The signal c_{ijk} follows Poisson statistics with the expectation value related to the classical intensity and written

$$\langle c_{ijk} \rangle = N \times \left[1 + V(\nu_j) \cos \left(\frac{2\pi i}{P_\Phi} s_\Phi + \frac{2\pi j}{P_\nu} s_\nu(k\tau) + \Phi(k\tau) \right) \right]. \tag{8}$$

Here, N is the expected photon count corresponding to an intensity of I_0 taking into account the quantum efficiency of the detector. One must be careful about the definitions of N and V, especially when comparing expressions for SNR in the literature, as they vary from paper to paper. In this work, the definition for V is given in Equation 1 while we will use several forms for the photon count N. With no subscript, N will denote the expected number of photon events in a single pixel during one sample. Adding subscripts to N will denote the sum over subsets of pixels. Thus N_ν is the expected number of counts in a single phase channel, summed across all the spectral pixels, while N_Φ denotes the expected number of counts in a single spectral channel, summed across all the phase pixels. The expected number of detected photon events across all pixels is written $N_{\nu\Phi}$. Since the spectral pixels are arranged evenly in wavenumber space, they will not necessarily contain the same average counts per cycle; however, a good approximation is that

$$N_{\nu\Phi} = P_\Phi \times N_\nu = P_\nu \times N_\Phi = P_\nu \times P_\Phi \times N. \tag{9}$$

When working through the SNR calculations, it is easiest to use the expected number of photon events in a single pixel N. However, when comparing these expressions it is best to use the number of events in an entire spectral channel N_Φ.

The angular brackets in Equation 8 denote an ensemble average, that is, if one could freeze the atmosphere and the OPD at their positions at time $k\tau$ and make multiple measurements we would find that c_{ijk} would follow Poisson statistics with an expected value given by Equation 8. The noise term r_{ijk} will be modeled as a Gaussian process with zero mean

and a standard deviation of σ. In the case of a CCD, σ corresponds directly to the readout noise figure.

Since the signal occurs at a single spatial frequency, either in the spectral pixels or in the phase pixels, a common way to approach the analysis of the signal is to perform a discrete Fourier transform (DFT) and look for a peak in the power spectrum. There will be $P_0/2$ channels of data in the power spectrum, where P_0 is either P_Φ or P_ν, and if the fringe spatial frequency corresponds exactly to one of these channels we can write the DFT of the signal as

$$|\Lambda(s)| = \begin{cases} N_0 & \text{for } s = 0 \\ N_0 V/2 & \text{for } s = s_0 \\ 0 & \text{otherwise} \end{cases} \tag{10}$$

where N_0 is either N_ν or N_Φ and s_0 is either s_ν or s_Φ depending on whether the DFT is taken across the spectral or phase direction of the detector. There will also be noise terms in this expression, and, if the fringe spatial frequency does not correspond exactly to a frequency bin of the DFT, spectral leakage will occur and the power will be spread amongst the adjacent harmonics. These matters will be taken up in a later section.

3. STATISTICAL METHODS

Both the signal term c_{ijk} and the noise term r_{ijk} follow standard statistical relationships. For the calculations that follow, we will require terms up to and including the fourth moment. In the case of the signal c_{ijk}, the following relationships apply

$$\begin{aligned} \langle c_{ijk}^2 \rangle &= \langle c_{ijk} \rangle^2 + \langle c_{ijk} \rangle \\ \langle c_{ijk}^3 \rangle &= \langle c_{ijk} \rangle^3 + 3\langle c_{ijk} \rangle^2 + \langle c_{ijk} \rangle \\ \langle c_{ijk}^4 \rangle &= \langle c_{ijk} \rangle^4 + 6\langle c_{ijk} \rangle^3 + 7\langle c_{ijk} \rangle^2 + \langle c_{ijk} \rangle. \end{aligned} \tag{11}$$

For the noise r_{ijk}, we have

$$\langle r_{ijk}^n \rangle = \begin{cases} (n-1)!!\,\sigma^n & \text{for } n \text{ even} \\ 0 & \text{for } n \text{ odd} \end{cases} \tag{12}$$

where we have used the standard notation

$$n!! = \begin{cases} 2 \times 4 \cdots \times n & \text{for } n \text{ even} \\ 1 \times 3 \cdots \times n & \text{for } n \text{ odd.} \end{cases} \tag{13}$$

We also note that the two parts, signal and noise, are statistically independent and so

$$\langle n_{ijk} \rangle = \langle c_{ijk} \rangle + \langle r_{ijk} \rangle \tag{14}$$

and

$$\langle c_{ijk}^n \, r_{ijk}^m \rangle = 0 \tag{15}$$

for $n \neq 0$ and $m \neq 0$.

In order to model the behavior of a measurement system, we introduce a second form of average to be denoted by a line above a variable:

$$\overline{\langle n_{ijk} \rangle} = \frac{1}{M} \sum_{k=1}^{k=M} \langle n_{ijk} \rangle. \tag{16}$$

This is an average across many samples, that is, the atmosphere and OPD are free to move and will almost certainly have different values during different samples. The integration time $M\tau$ is chosen such that the projected baseline does not change significantly and cause baseline smearing.

When analyzing a particular measurement system to find its expected value or some statistical moment, one must be careful to expand the expression completely in terms of the ensemble average first, using Equations 11, 12, 14, and 15 and then to analyze the time averaged statistics. This is equivalent to ensuring that you know what is going on in a single sample before considering many samples. So, for example, consider the expected value of the counts in one pixel averaged over time:

$$\begin{aligned}
\overline{\langle n_{ijk}\rangle} &= \overline{\langle c_{ijk}\rangle} + \overline{\langle r_{ijk}\rangle} \\
&= \frac{1}{M}\sum_{k=1}^{k=M} N \times \left[1 + V(\nu_j)\,\cos\left(\frac{2\pi i}{P_\Phi}s_\Phi + \frac{2\pi j}{P_\nu}s_\nu(k\tau) + \Phi(k\tau)\right)\right] + 0 \\
&= N \times \left[1 + V(\nu_j)\,\frac{1}{M}\sum_{k=1}^{k=M}\cos\left(\frac{2\pi i}{P_\Phi}s_\Phi + \frac{2\pi j}{P_\nu}s_\nu(k\tau) + \Phi(k\tau)\right)\right] \\
&= N
\end{aligned} \tag{17}$$

as one would expect. The time averaged value of the cosine function goes to zero since, due to residual atmospheric turbulence, the phase term $\Phi(k\tau)$ takes on a different and random value each cycle if phase locking is not used. For the higher order moments, we will also need to consider time averages of the cosine function. We will again assume that the atmospheric term takes on a different and random value during each sample period and so

$$\begin{aligned}
\overline{\cos^n\left(\frac{2\pi i}{P_\Phi}s_\Phi + \frac{2\pi j}{P_\nu}s_\nu(k\tau) + \Phi(k\tau)\right)} &\approx \frac{1}{2\pi}\int_0^{2\pi}\cos^n x\,dx \\
&= \begin{cases} \frac{(n-1)!!}{n!!} & \text{for } n \text{ even} \\ 0 & \text{for } n \text{ odd.} \end{cases}
\end{aligned} \tag{18}$$

The other statistical distributions that will be required for the analysis of fringe tracking are the Rayleigh and Rician probability density functions. These were first used by Walkup & Goodman (1973) and represent, respectively, the noise probability density function and the signal plus noise probability density function of the DFT of the fringe signal shown in Equation 10. The frequency channels of the DFT not corresponding to the fringe spatial frequency follow the Rayleigh distribution, while the channel that does correspond to the fringe spatial frequency follows the Rician distribution. These two distributions are related and can be written

$$P(Z,s) = \frac{Z}{\sigma_Z^2}\exp\left[-\frac{1}{2\sigma_Z^2}(Z^2 + |\Lambda(s)|^2)\right] I_0\left(\frac{|\Lambda(s)|Z}{\sigma_Z^2}\right) \tag{19}$$

where $I_0(x)$ is the modified Bessel function of order zero. The second moment of the distribution is

$$\langle Z^2\rangle = |\Lambda(s)|^2 + 2\sigma_Z^2. \tag{20}$$

4. CORRELATION MEASUREMENT

The primary goal of an interferometer is to measure $|\gamma(\nu_j)|$, the visibility magnitude at a given wavelength at the current projected baseline. In order to do this, we measure the apparent visibility $V(\nu_j)$ and calibrate for the coherence transfer factor $\eta(\nu_j)$ by switching between an unresolved, or well known, object and the object of scientific interest. There are many methods for measuring V, almost all of which result in an estimate for V^2, called the correlation. Each method, however, has a slightly different form for the SNR. In this paper, we will consider three methods in detail: the method first proposed by Tango & Twiss (1980), a method based on the DFT, and a modified version of the Tango & Twiss method.

SNR expressions exist for the case of a noiseless detector along with methods for compensating for photon noise in the measurement. With the addition of noise in the detector, the signal is further corrupted and the effects of detector noise must be subtracted out. Thus one must know the value of σ in order to calibrate the measurements made. In the derivations that follow, we will consider two cases: one in which the detector noise is well known in advance of the correlation measurement, which we shall refer to as the "known-noise" case, and one in which we are estimating σ with the same data as that used to estimate the correlation $V(\nu_j)$, which we shall refer to as the "unknown-noise" case. In general, the known-noise case produces a better SNR than does the unknown-noise case; however, the former relies on knowing the noise properties of the detector in advance, something that will not always be the case. Since a correlation measurement is made independently in each spectral channel, in many places the j subscripts will be removed for the sake of notational clarity.

4.1. The Tango & Twiss Method

The method described by Tango & Twiss (1980) involves a single pixel detector on either side of the beam splitter while inserting a quarter-wave plate into one beam every other cycle. This is similar to the example configuration shown in Figure 1 and is equivalent to setting $P_\Phi = 4$ and $s_\Phi = 1$. The measurement technique used on the Mark III interferometer (Shao et al. 1988) involves integrating over the fringes in four phase bins, but is essentially the same.

We form the biased and unnormalized estimate for the kth sample in the jth spectral channel

$$q_k = (n_{1k} - n_{3k})^2 + (n_{2k} - n_{4k})^2 \tag{21}$$

with the expectation value over many samples of

$$\overline{\langle q \rangle} = 4N^2V^2 + 4N + 4\sigma^2 \tag{22}$$

which represents a measurement of the signal power plus the noise power. We can estimate the photon noise power by summing the counts in all four phase pixels, and we find that

$$\overline{\left\langle \sum_{i=1}^{4} n_i \right\rangle} = 4N \tag{23}$$

which can be subtracted from our biased estimator $\overline{\langle q_j \rangle}$ to remove the effects of photon noise. The detector noise term $4\sigma^2$, however, still needs to be removed. If we know the

detector's noise characteristics in advance, this can be done easily. We thus arrive at the "known-noise" unbiased estimator

$$\overline{\langle C^2 \rangle} = \overline{\langle q \rangle} - \overline{\langle \sum_{i=1}^{4} n_i \rangle} - 4\sigma^2 = 4N^2V^2. \tag{24}$$

This still needs to be normalized to yield the normalized estimator

$$\overline{\langle C_N^2 \rangle} = \frac{\overline{\langle C^2 \rangle}}{4N^2} = V^2. \tag{25}$$

To calculate the SNR of this estimate we must first calculate its variance. We start by calculating the variance of the unnormalized estimator using

$$\mathrm{VAR}(\langle C^2 \rangle) = \mathrm{VAR}(\langle q \rangle) + \mathrm{VAR}(\langle \textstyle\sum_{i=1}^{4} n_i \rangle) - 2 \times \mathrm{COVAR}(\langle q \rangle, \langle \textstyle\sum_{i=1}^{4} n_i \rangle). \tag{26}$$

The variances and covariances in Equation 26 can be calculated in a manner similar to the example calculation given in Equation 17, and we find that

$$\mathrm{VAR}(\langle q \rangle) = 32N^3V^2 + 16N^2(1 + V^2) + 4N + 32\sigma^2(N^2V^2 + N) + 16\sigma^4, \tag{27}$$

$$\mathrm{VAR}(\langle \textstyle\sum_{i=1}^{4} n_i \rangle) = 4N + 4\sigma^2 \tag{28}$$

and

$$\mathrm{COVAR}(\langle q \rangle, \langle \textstyle\sum_{i=1}^{4} n_i \rangle) = 8N^2V^2 + 4N. \tag{29}$$

Combining Equations 26, 27, 28, and 29 results in

$$\mathrm{VAR}(\langle C^2 \rangle) = 32N^3V^2 + 16N^2 + \sigma^2(32N^2V^2 + 32N + 4) + 16\sigma^4. \tag{30}$$

To find the variance of the normalized correlation estimator, we divide Equation 30 by $16N^4$. This step implies that we know the value of N exactly, an assumption that has been made implicitly in all previously published SNR calculations. While this is not strictly true, it is a fairly good approximation provided that the number of samples in the measurement is relatively large. The SNR of a signal is the expected signal value divided by its standard deviation, and so we have

$$\mathrm{SNR}(V^2) = \frac{\sqrt{M}N^2V^2}{\sqrt{2N^3V^2 + N^2 + \sigma^2(2N^2V^2 + 2N + \frac{1}{4}) + \sigma^4}}. \tag{31}$$

This can be compared to previous SNR calculations if one puts $\sigma = 0$ and is careful about the definitions of N and V. We shall call this the "known-noise Tango & Twiss" estimator SNR. In order to compare this to other SNR expressions we recall that $N_\Phi = 4N$ in this system resulting in

$$\mathrm{SNR}(V^2) = \frac{\sqrt{M}N_\Phi^2V^2}{4\sqrt{N_\Phi^2 + \frac{1}{2}N_\Phi^3V^2 + 8\sigma^2(\frac{1}{4}N_\Phi^2V^2 + N_\Phi + \frac{1}{2}) + 16\sigma^4}}. \tag{32}$$

If the detector noise properties are not well known or change with environmental conditions, this measurement method will not work. Instead, we need to estimate the readout noise

at the same time as estimating the signal correlation. This can be done by simultaneously calculating

$$\overline{\langle(\sum_{i=1}^{4} n_i)^2\rangle} = 16N^2 + 4N + 4\sigma^2 \tag{33}$$

and forming the unbiased estimator

$$\overline{\langle C^2\rangle} = \overline{\langle q\rangle} - \overline{\langle(\sum_{i=1}^{4} n_i)^2\rangle} = 4N^2(V^2 - 4) \tag{34}$$

resulting in the normalized estimator

$$\overline{\langle C_N^2\rangle} = \frac{\overline{\langle C^2\rangle}}{4N^2} + 4 = V^2. \tag{35}$$

This has a SNR given by

$$\mathrm{SNR}(V^2) = \frac{\sqrt{M}N^2V^2}{4\sqrt{\frac{1}{4}N_\Phi^3(16 - 6V^2) + N_\Phi^2(4 - V^2) + \sigma^2[N_\Phi^2(16 + 2V^2) + 24N_\Phi] + 64\sigma^4}}, \tag{36}$$

and we shall refer to it as the "unknown-noise Tango & Twiss" estimator.

An inspection of Equations 32 and 36 makes it clear that the known-noise estimator will always have a better SNR than the unknown-noise estimator. However, it is likely that the unknown-noise estimator will produce more reliable results in the long term because the noise characteristics of the detector evolve with time and environmental conditions.

It will be useful to know how these expressions behave in the limits of very large and very small photon counts, although it is the low light levels that will be of most interest. The high light level limit is independent of the detector noise and is

$$\mathrm{SNR}(V^2) \approx \frac{1}{2}\sqrt{\frac{MN_\Phi}{2}}V. \tag{37}$$

For low light levels, there are different approximations for the noiseless and noisy cases. For a noiseless detector

$$\mathrm{SNR}_{\mathrm{noiseless}}(V^2) \approx \frac{\sqrt{M}V^2N_\Phi}{4} \tag{38}$$

while for a noisy detector

$$\mathrm{SNR}_{\mathrm{noisy}}(V^2) \approx \frac{\sqrt{M}N_\Phi^2V^2}{\mathcal{X}\sigma^2} \tag{39}$$

where $\mathcal{X} = 16$ for the known-noise case and $\mathcal{X} = 32$ for the unknown-noise case.

4.2. Discrete Fourier Transform

If the phase dimension of the detector has at least 4 pixels, one can use the DFT set out in Equation 10 to estimate the visibility. In most practical systems, the fast Fourier Transform (FFT) is used but this does not affect the results. In the case of the bin that corresponds to the spatial frequency of the fringes, $s = s_\Phi$ and the total power is the signal power given in Equation 10 plus the noise power. The noise power is the sum of the variances of the two sources of noise, photon statistics and detector noise. The variance of the photon events is N_Φ while the variance of the detector noise will be $N_\Phi\sigma^2$. Frequency bins that do not

correspond to the fringe spatial frequency will contain only noise power. This means that the power spectrum will have the form

$$\overline{\langle|\Lambda_\Phi(s)|^2\rangle} = \begin{cases} N_\Phi^2 + N_\Phi + N_\Phi\sigma^2 & \text{for } s = 0 \\ N_\Phi^2 V^2/4 + N_\Phi + N_\Phi\sigma^2 & \text{for } s = s_\Phi \\ N_\Phi + N_\Phi\sigma^2 & \text{otherwise.} \end{cases} \tag{40}$$

Once the noise power is subtracted, the signal in the $s = s_\Phi$ bin is a correlation measurement. We measure and remove the noise power in the same way as described above for the known-noise Tango & Twiss estimator.

The SNR of this measurement of fringe visibility for the "known-noise" case is given by Beletic (1994) as

$$\mathrm{SNR}(V^2) = \frac{\sqrt{M} N_\Phi^2 |T(\nu_j)|^2 |\gamma(\nu_j)|^2}{\sqrt{N_\Phi^2 + 2N_\Phi^3 |T(\nu_j)|^2|\gamma(\nu_j)|^2 + 2P_\Phi\sigma^2(N_\Phi^2|T(\nu_j)|^2|\gamma(\nu_j)|^2 P_\Phi\sigma^4 + N_\Phi) + P_\Phi^2\sigma^4}} \tag{41}$$

where $T(\nu_j)$ is the normalized optical system transfer function.

In order to measure V^2 with the DFT, we need to set $|T(\nu_j)| = \eta/2$, which yields

$$\mathrm{SNR}(|\Lambda|^2) = \frac{\sqrt{M}|\Lambda|^2}{\sqrt{N_\Phi^2 + 2N_\Phi|\Lambda|^2 + 2P_\Phi\sigma^2(|\Lambda|^2 + N_\Phi) + P_\Phi^2\sigma^4}}. \tag{42}$$

We can put this into a similar form to the Tango & Twiss estimators by recalling that $|\Lambda|^2 = N_\Phi^2 V^2/2$, resulting in an SNR for the visibility measurement of

$$\mathrm{SNR}(V^2) = \frac{\sqrt{M} N_\Phi^2 V^2}{4\sqrt{N_\Phi^2 + \frac{1}{2}N_\Phi^3 V^2 + 2P_\Phi\sigma^2(\frac{1}{4}N_\Phi^2 V^2 + N_\Phi) + P_\Phi^2\sigma^4}}. \tag{43}$$

Putting $P_\Phi = 4$ makes this the same as the Tango & Twiss known-noise estimator SNR given in Equation 32, except for the extra factor of $\frac{1}{2}$ in the denominator of the Tango & Twiss formula. Thus we can say that the Tango & Twiss estimator is an example of the DFT across 4 pixels.

In the high photon count limit, as with the Tango & Twiss method, this expression can be approximated by $\frac{1}{2}\sqrt{\frac{MN}{2}}V$ for both a noiseless and a noisy detector. For a noiseless detector at low light levels

$$\mathrm{SNR}_{\mathrm{noiseless}}(V^2) \approx \frac{\sqrt{M} V^2 N_\Phi}{4} \tag{44}$$

while for a noisy detector

$$\mathrm{SNR}_{\mathrm{noisy}}(V^2) \approx \frac{\sqrt{M} N_\Phi^2 V^2}{4P_\Phi\sigma^2}. \tag{45}$$

4.3. Modified Tango & Twiss Method

Based on the expressions for SNR above, it is clear that the SNR for a noisy detector deteriorates very quickly with an increase in the number of pixels. Thus to achieve the

best SNR, we should use as few pixels as possible. The Tango & Twiss method outlined in Section 4.1 produces a correlation estimate for every sample and uses four pixels. It can also be used to supply an estimate for the fringe phase every cycle. If we forgo these features, it is possible to produce a correlation estimator that uses only two pixels and thereby achieve a better SNR, which we shall call the "modified Tango & Twiss method". For this method to work, we must assume that the atmosphere changes the fringe phase randomly and the cosine terms average out according to Equation 18. This was the method used in the Sydney University Stellar Interferometer (SUSI) prototype and, at the time of writing, the SUSI (Davis et al. 1994) instrument itself. In this measurement scheme, $P_\Phi = 2$ and, as before, $s_\Phi = 1$, which is equivalent to a single pixel per spectral channel on either side of a beam splitter. The biased and unnormalized estimator then becomes

$$q_k = (n_{1k} - n_{2k})^2 \tag{46}$$

which has the expectation over many samples of

$$\overline{\langle q \rangle} = 2N^2V^2 + 2N + 2\sigma^2. \tag{47}$$

Once again we must subtract out the noise power terms $2N$ and $2\sigma^2$. The known-noise and unknown-noise cases are similar to the Tango & Twiss method described above. In the known-noise case we use

$$\overline{\langle C^2 \rangle} = \overline{\langle q \rangle} - \overline{\langle \textstyle\sum_{i=1}^{4} n_i \rangle} - 2\sigma^2 = 2N^2V^2 \tag{48}$$

resulting in the normalized correlation estimator

$$\overline{\langle C_N^2 \rangle} = \frac{\overline{\langle C^2 \rangle}}{2N^2} = V^2. \tag{49}$$

Recalling that in this case $N_\Phi = 2N$, this has a SNR of

$$\mathrm{SNR}(V^2) = \frac{\sqrt{M} N_\Phi^2 V^2}{4\sqrt{\frac{1}{32}N_\Phi^4V^4 + \frac{1}{2}N_\Phi^3V^2 + \frac{1}{2}N_\Phi^2 + \sigma^2(N_\Phi^2V^2 + 2N_\Phi + \frac{1}{2}) + 2\sigma^4}}. \tag{50}$$

If the detector noise properties are not well known in advance, or vary in time or across pixels, we need to use the unknown-noise estimator

$$\overline{\langle C^2 \rangle} = \overline{\langle q \rangle} - \overline{\langle (\textstyle\sum_{i=1}^{4} n_i)^2 \rangle} = 2N^2(V^2 - 2) \tag{51}$$

resulting in the normalized estimator

$$\overline{\langle C_N^2 \rangle} = \frac{\overline{\langle C^2 \rangle}}{2N^2} + 2 = V^2 \tag{52}$$

which has a SNR of

$$\mathrm{SNR}(V^2) = \frac{\sqrt{M} N_\Phi^2 V^2}{4\sqrt{\frac{1}{32}N_\Phi^4V^4 + (N_\Phi^3 + N_\Phi^2)(1 - \frac{1}{2}V^2) + 2\sigma^2[N_\Phi^2(1 + \frac{1}{2}V^2) + 2N_\Phi] + 4\sigma^4}}. \tag{53}$$

In contrast to the other correlation estimators, the SNR in a single sample does not always increase with increasing photon events. In fact, for both Equation 50 and Equation 53 we find that

$$\lim_{N\to\infty} \mathrm{SNR}(V^2) = \sqrt{2M}. \tag{54}$$

For the low photon count levels we have for a noiseless detector

$$\mathrm{SNR}_{\mathrm{noiseless}}(V^2) \approx \frac{1}{2}\sqrt{\frac{M}{2}} N_\Phi V^2, \tag{55}$$

while for a noisy detector

$$\mathrm{SNR}_{\mathrm{noisy}}(V^2) \approx \frac{\sqrt{M} N_\Phi^2 V^2}{\mathcal{X}\sigma^2} \tag{56}$$

where $\mathcal{X} = 4\sqrt{2}$ in the known-noise case and $\mathcal{X} = 16$ for the unknown-noise case.

4.4. Comparison

It remains to compare these different correlation estimates. It is clear from the above analysis that the SNR is a strong function of pixel number for a noisy detector. Thus, when measuring signal correlation it is most advantageous to pick the measurement scheme that uses the least number of pixels. The DFT method uses the greatest number of pixels, and furthermore requires that the spatial frequency of the fringes across the phase dimension of the detector falls exactly into one of the frequency bins in the power spectrum. If this is not the case, spectral leakage will spread the signal energy amongst several pixels, reducing the SNR. This is difficult to do, especially if many spectral channels are desired. Most methods of introducing the phase changes across a detector, like adding a constant tilt or combination in the image plane, are wavelength dependent. The Tango & Twiss method is basically equivalent to a DFT with four pixels. Because this can be done by using a simple beam splitter, thereby ensuring the correct phase relationships, the Tango & Twiss method does not suffer from these problems. We will therefore not consider the DFT method in the following analysis.

Figure 2 contains a number of plots of the predicted SNR in a single sample as a function of detected photon events for various visibilities and detector noise values. The value of $\sigma = 6$ has been chosen as a value for production CCD detector arrays. We will also use a value of $\sigma = 3$ in some calculations, which represents a 'current best' value for CCDs. As one would expect, a noiseless detector system achieves the best SNR for any given photon count. These plots also show that the modified Tango & Twiss measurement scheme performs the best at low count rates, while it goes to $\sqrt{2M}$ for high count rates as per Equation 54. This holds true for both the known-noise and unknown-noise cases. For correlation measurements then, the modified Tango & Twiss estimator is preferable whether one is using a noisy detector or not.

In order to compare the noisy case with the noiseless case we must also take into account the DQE of the different types of detector. Figure 3 contains plots of predicted SNR and predicted integration times for the noiseless and the known-noise modified Tango & Twiss estimator, where in the case of the noiseless detector the DQE has been set to 10% and for the noisy detector the DQE has been set to 80%. The 10% figure is higher than any currently available photon noise limited array detector, while the 80% figure is slightly lower than the best DQE's reported for a CCD. The topmost plot in Figure 3 shows the predicted

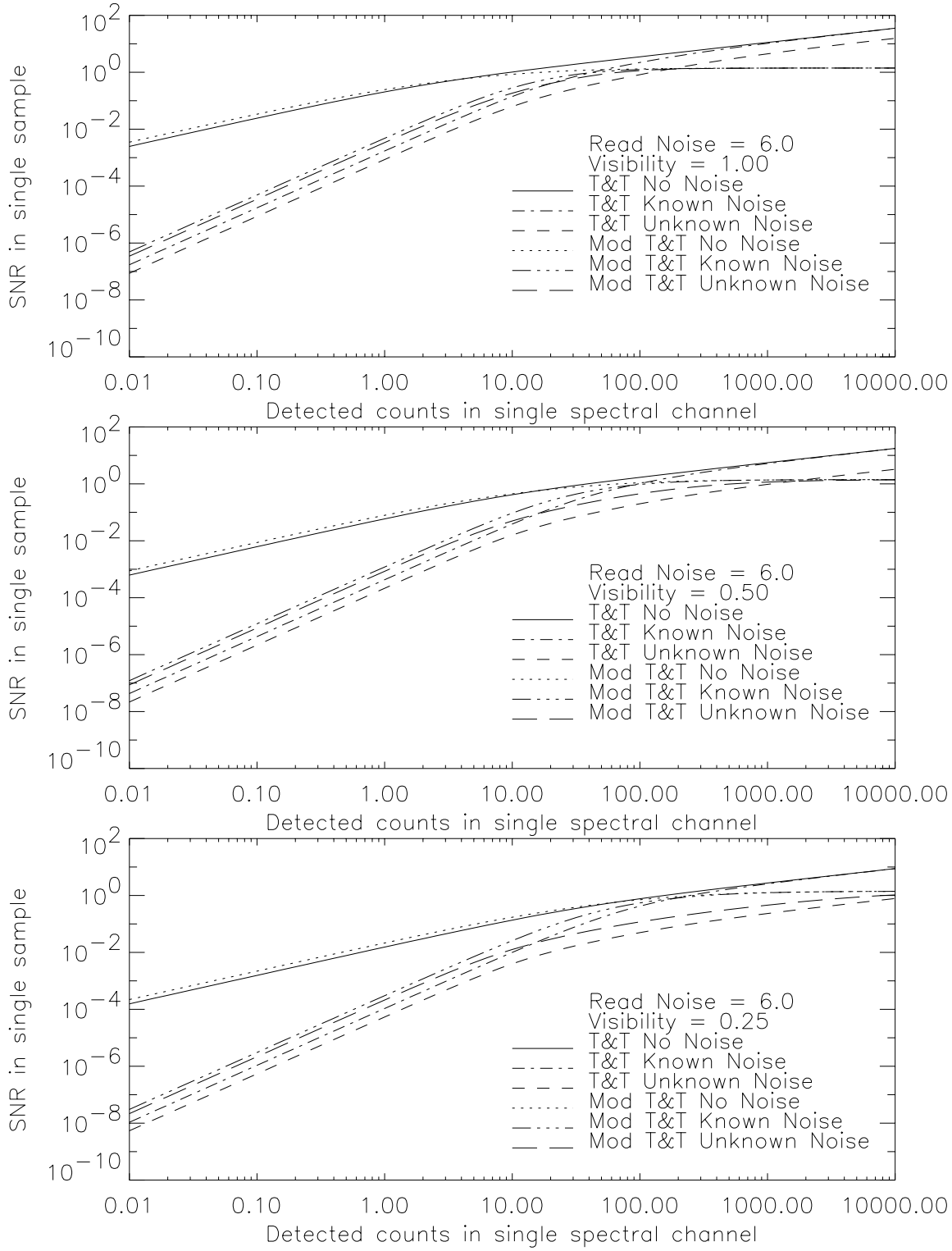

FIGURE 2. Plots of SNR for the Tango & Twiss and Modified Tango & Twiss measurement methods for a range of visibilities and a noise value of 6.

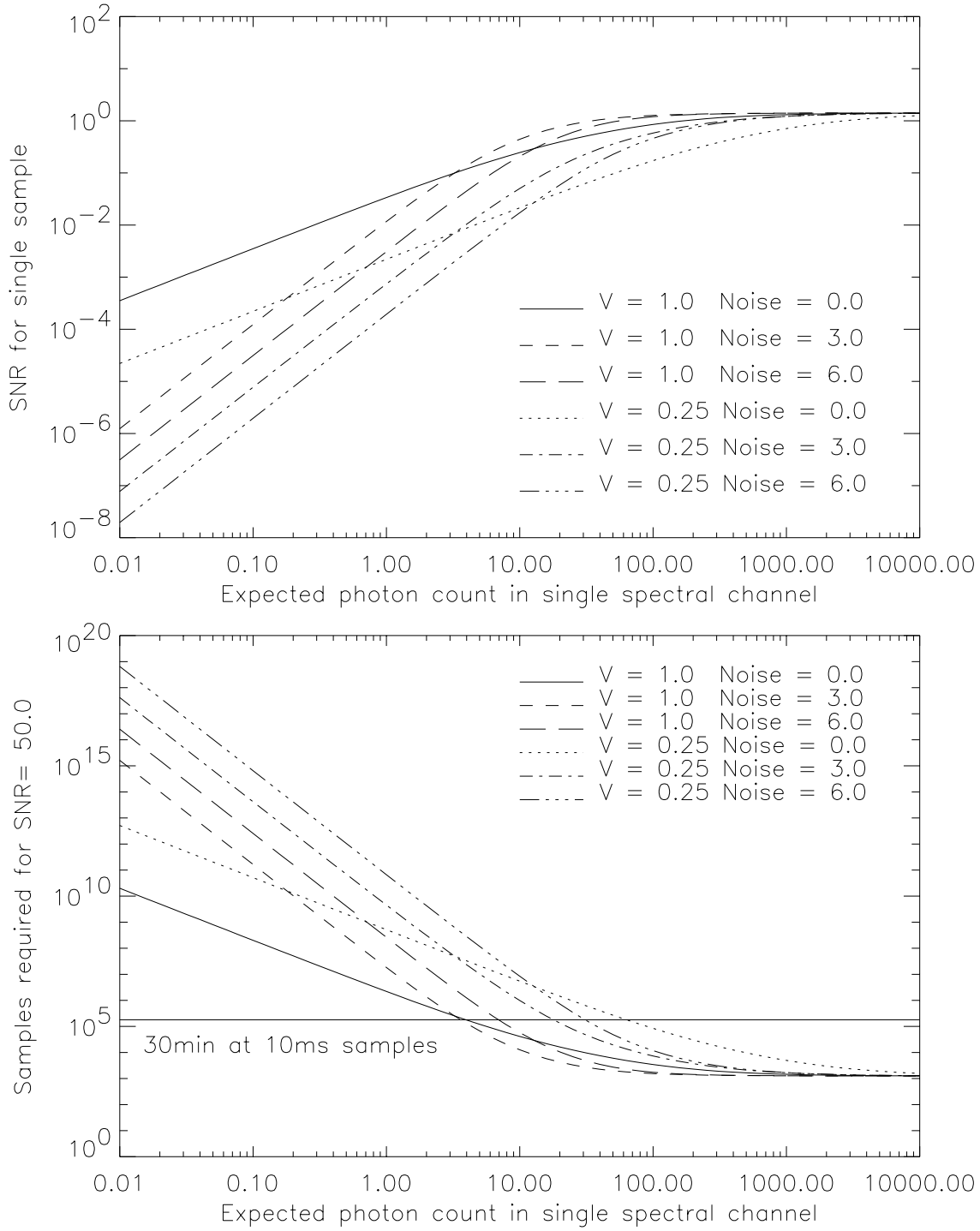

FIGURE 3. Comparison of a noiseless and noisy detector using the known-noise modified Tango & Twiss method. The top plot shows the expected SNR while the bottom plot shows the number of samples required for a total SNR of 50. The noiseless detector is assumed to have a DQE of 10% while the noisy detector has a DQE of 80%.

SNR for visibilities of 1 and 0.25. At the lowest count rates, the noiseless detector has the best performance. This will always be true even if the noisy detector were 100% efficient. However, the noisy detector has a better SNR for a substantial range of count rates. The crossover point occurs at $N_\Phi \approx 3$ when $\sigma = 3$ and at $N_\Phi \approx 10$ when $\sigma = 6$ for both visibilities.

Another way of comparing the detectors is shown in the lower plot of Figure 3. This plot contains the same data except the vertical axis now represents the number of samples required in an integration to achieve a SNR of 50. An horizontal line has also been added representing an half-hour integration for a sample time of 10 ms. In the case of a visibility of 1, it is only at this point that the noiseless detector starts to be a better choice than the noisy detector, for both the $\sigma = 3$ and the $\sigma = 6$ cases. For lower visibilities, this does not occur until integrations several orders of magnitude longer are used, by which time the projected baseline will have changed significantly. The measured visibility will always be less than one. Thus in terms of required integration times for a given SNR, a noisy detector may be quite adequate for correlation measurement. For example, for an aperture size of 20 cm, the sample time of 10 ms quoted above, an optical system throughput of 5% and an optical bandwidth of 3nm a noisy detector will have magnitude limit of 8 in the case of $V = 1$ after an half-hour integration, the same as that of the noiseless detector. For the $V = 0.25$ case, the magnitude limits are 6 for $\sigma = 3$, 5.5 for $\sigma = 6$ and 4.7 for the noiseless detector. While using a high-DQE single-pixel photon noise limited detector, such as an APD, would achieve better magnitude limits, if one already has an array detector available (like a CCD), the latter could be used for correlation measurement.

5. GROUP DELAY TRACKING

The fringe envelope must be located and tracked before any correlation measurements can be made, and, unless some form of passive interferometry is used, the fringe tracking system will define the magnitude limit of the instrument. Fringe tracking can take two forms: phase locking, where the tracking servo loop is closed to within a fraction of the fringe phase, or group delay tracking (GDT), which is less precise and tracks to within a fraction of the fringe envelope. In this analysis we shall use GDT for several reasons. First, phase locking requires at least four pixels in the phase dimension of the detector, either by using a temporal encoding scheme like that used in the Mark III or with wave-plates as in the Tango & Twiss method. This means phase tracking is wavelength dependent, requires many pixels, and, given the same DQE, will have a brighter magnitude limit than GDT. In contrast, GDT requires only a single phase pixel in each spectral channel. Secondly, when phase locking fails, it does so catastrophically, while GDT can be used for passive tracking and post-processing even if it has failed for actively tracking the fringe envelope. Finally, in order for some of the correlation measurement schemes to work, we have assumed that a residual phase error occurs due to the atmosphere. This will not be true for phase locking.

Group delay tracking relies on the fact that the spatial frequency of the fringes in the spectral dimension of the detector is linearly related to the OPD. In order to find this spatial frequency we calculate a DFT across the spectrum, which gives us

$$\overline{\langle |\Lambda_\nu(s)|^2 \rangle} = \begin{cases} N_\nu^2 + N_\nu + N_\nu\sigma^2 & \text{for } s = 0 \\ N_\nu^2 V^2/4 + N_\nu + N_\nu\sigma^2 & \text{for } s = s_\nu \\ N_\nu + N_\nu\sigma^2 & \text{otherwise} \end{cases} \tag{57}$$

and search for a peak. The frequency bin containing this peak should be that corresponding

to $s = s_\nu$, and Equation 4 can then be used to find the OPD. This will fail to give the correct result if the noise causes the highest peak to be in a frequency bin other than $s = s_\nu$. Thus the SNR of the DFT estimator is not as important in fringe tracking as the probability that some noise peak will be higher than the signal peak. In this analysis we shall follow the work by Lawson (1994), in which a complete description of the GDT method using a photon noise limited detector can be found.

In a single sample, the amplitude of the signal plus noise and the noise by itself follow the Rician and Rayleigh distribution given in Equation 19, where we use Equation 10 to define $|\Lambda(s)|$ and, due to the similarities of Equation 57 to Equation 20, we set

$$2\sigma_Z^2 = N_\nu + N_\nu\sigma^2. \tag{58}$$

In the case of a power spectrum averaged over many samples we must use joint-probability distributions. For M samples these joint-probability distributions are found by convolving the Rician and Rayleigh distributions with themselves M times. The probability that at least one noise peak amongst b channels is higher than the signal peak is given by

$$p_e = 1 - \int_0^\infty P(Z, s = s_\nu) \left[\int_0^Z P(z, s \neq s_\nu)dz\right]^b dZ. \tag{59}$$

An important consideration when performing this calculation is the choice of a value for b. If the fringe location is totally unknown, the value of b must be set to the number of frequency bins in the DFT. If it is known that the fringes could not have moved more than a small distance since the last measurement, the value of b can be reduced. Furthermore, if b is large, the internal integral in Equation 59 raised to this power is likely to be a number either too small or too large to be accurately represented in computer memory. These matters as well as methods for calculating these probabilities numerically are outlined in the paper by Lawson (1994).

Several examples of tracking loss probability curves are shown in Figure 4 for channeled spectra with $N_\nu = 256$ and a measured visibility of 0.5. The search for a peak is across all pixels in the DFT excluding the zero frequency or DC channel, and so $b = 127$. The calculations have been performed for three levels of noise: $\sigma = 0$, $\sigma = 3$ and $\sigma = 6$; and for integrations across 1, 10, 100 and 1000 samples. In each case, the DQE of the detector has been set to 100%. The addition of detector noise has two effects. The first, and most detrimental, is to increase the number of detected photon events required to maintain tracking. The second effect is an increased slope in the probability of tracking loss with reduced photon counts. This second effect is similar to changing the b parameter.

As with the comparison of correlation measurements in Section 4.4, a more practical way to judge the effect of detector noise is to take into account the difference in DQE of the two types of detector. Several sets of probability curves have been plotted in Figure 5 for a range of integration times and visibility values of 0.25, 0.5 and 1.0. Once again the DQE of the noiseless detector has been set to 10% and that of the noisy detector to 80% with a noise level of $\sigma = 3$. These represent best cases for an intensified CCD or photon counting array like a PAPA camera (Papaliolios & Mertz 1981) and a modern bare CCD. For the highest visibility levels and longest integration times, the noiseless detector still has the best performance. However, unresolved objects will never be the major target of a stellar interferometer. At the lower visibilities and shorter integration times the noisy detector starts to out-perform the noiseless detector, with the only disadvantage being the increased slope of the curve implying that failure will be more catastrophic. If we take

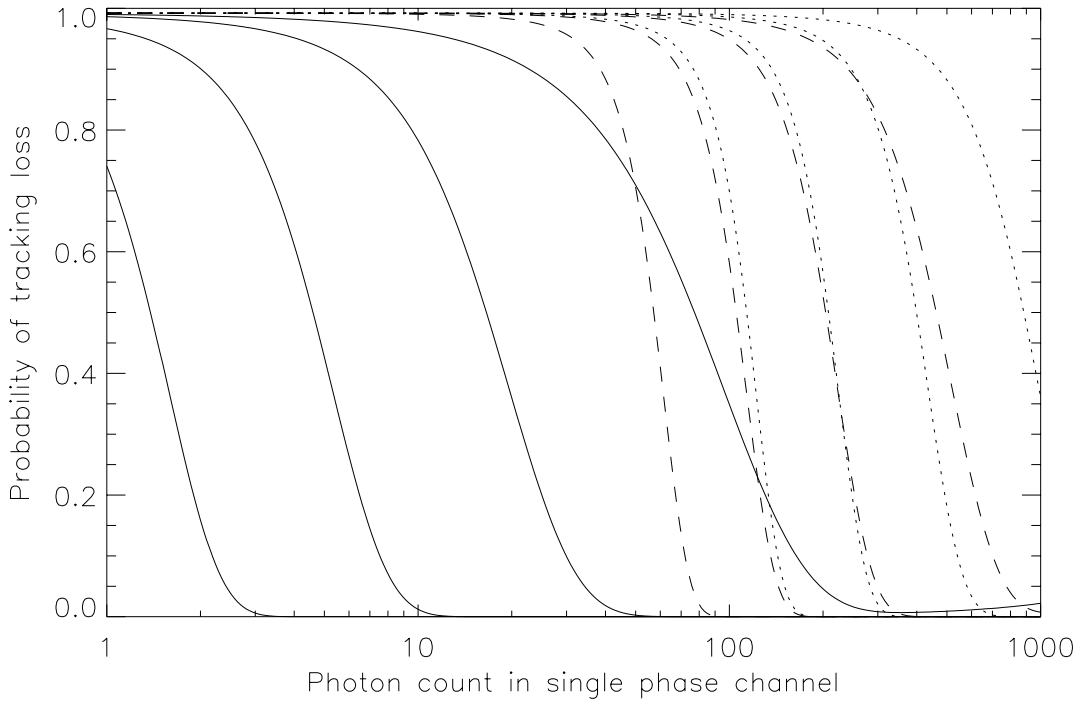

FIGURE 4. The probability of tracking failure for a visibility of 0.5 measured across 256 pixels and setting $b = 127$ (all DFT pixels except the DC channel) with no noise (solid lines), a noise of $\sigma = 3$ (dashed lines) and noise of $\sigma = 6$ (dotted lines). Four integration times are shown for each noise level which are from right to left: $M = 1$, $M = 10$, $M = 100$ and $M = 1000$.

into account the other features of a CCD — relatively low cost, flexibility due to noiseless on-chip rebinning, and large optical bandwidth — it becomes an attractive device for use in group delay tracking. Furthermore, if the number of pixels N_ν is reduced, the effect of detector noise is reduced, making a high-DQE, noisy detector even more promising.

As an illustration of the potential of a noisy detector, consider tracking an object whose measured visibility at the current baseline and atmospheric conditions is 0.5. Using the same sample time of 10 ms, aperture size of 20 cm, and optical throughput of 5% used in Section 4.4, together with the optical configuration shown in Figure 1, it is possible to estimate the magnitude limit of fringe tracking. Since there is a spectrum available on both sides of the beam splitter, two channeled fringes are available, and the probability of tracking loss may be squared, reflecting the likelihood that both channels lose the fringe signal. Table 1 contains the magnitudes at which the probability of tracking loss is 1%, once again using the 10% and 80% DQE figures for the noiseless and noisy detectors and setting $N_\Phi = 64$ and $b = 31$. The noisy detector has a higher magnitude limit in all cases. As the integration M is increased the effects of detector noise increases, reflecting the fact that many 'readouts' of the detector are required. At high values of M, the noiseless detector starts to out-perform the noisy detector. However, for active fringe tracking, a detector capable of tracking in the shortest possible integration time is desired. Clearly a noisy detector such as a CCD is suitable for group delay tracking and, if a large aperture were broken up into multiple subapertures, even fainter objects could be targeted.

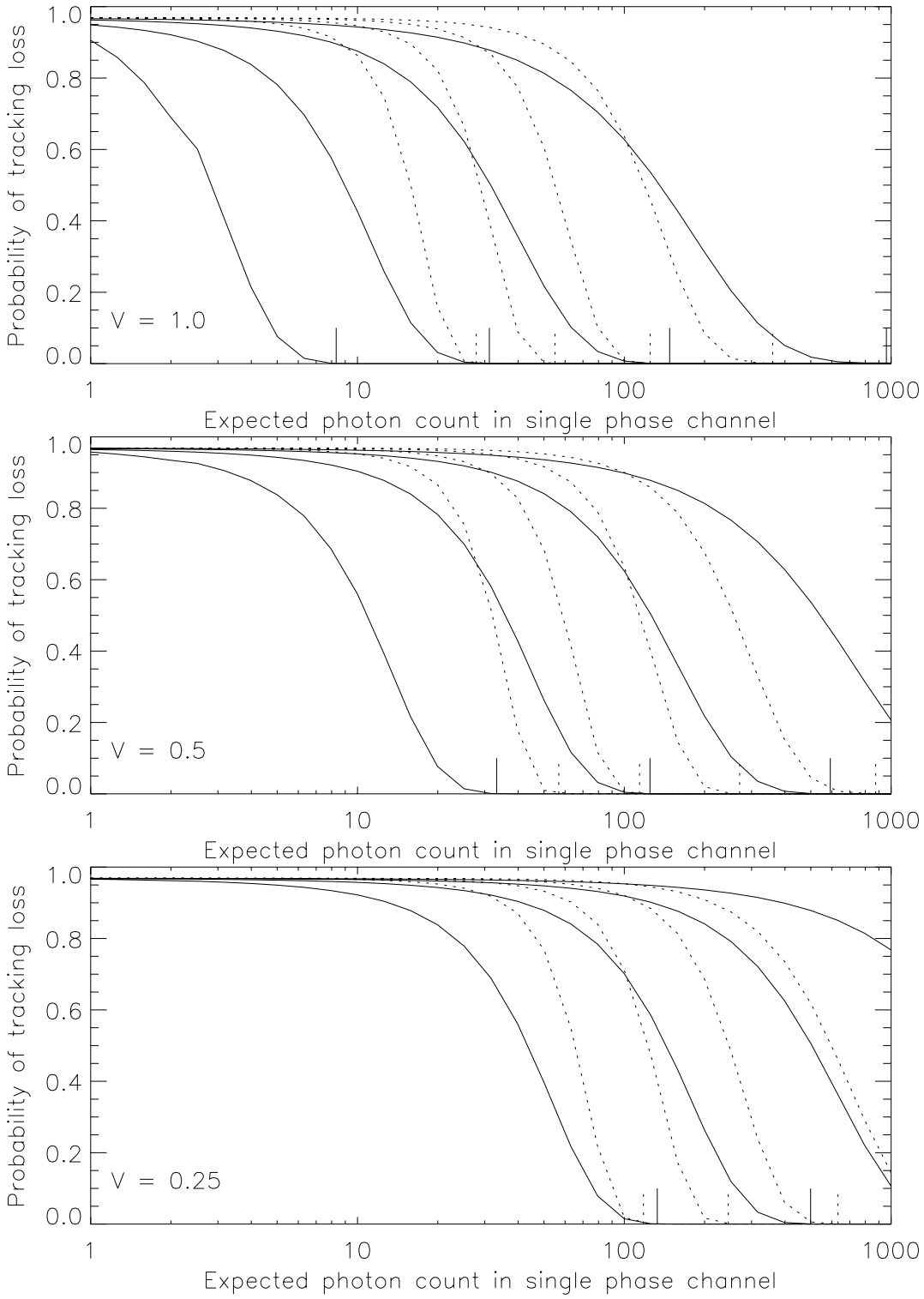

FIGURE 5. Probability of tracking loss for a range of visibilities. The solid lines represent a 10% noiseless detector while the dashed lines represent an 80% detector with $\sigma = 3$. From right to left, the plots are for $M = 1$, $M = 10$, $M = 100$ and $M = 1000$. The short vertical lines along the horizontal axis are the approximated tracking failure points.

TABLE 1. Fringe tracking magnitude limits for noiseless and noisy detectors.

	DQE = 10%	DQE = 80%	
M	$\sigma = 0$	$\sigma = 3$	$\sigma = 6$
1	6.6	7.8	7.2
10	8.4	8.9	8.2

5.1. Gaussian approximation

The numerical calculation of the integrals in Equation 59 are time consuming. Because one is typically more interested in the point at which the probability is significantly greater than zero, and not the exact probability for all light levels, it is useful to have an approximate form for the point of tracking failure. In the limit of large values of M, both the Rician and Rayleigh distributions are well approximated by a Gaussian with the mean value of $|\Lambda(s)|^2$ and a variance given by the variance of the $|\Lambda(s)|^2|$ estimator. In the case of group delay tracking, the estimator is the DFT. Thus we can use a Gaussian probability over $Z(s)$ and set the mean to

$$\overline{Z(s)} = |\Lambda(s)|^2 \tag{60}$$

where for the pixel containing the fringe signal $|\Lambda(s = s_\nu)| = NV/2$ and for all other pixels $|\Lambda(s \neq s_\nu)| = 0$. Following Equation 42, we set the variance of both the signal plus noise pixel and the noise only pixels to

$$\sigma^2_{Z(s)} = \frac{1}{M}[N_\Phi^2 + 2N_\Phi|\Lambda|^2 + 2P_\Phi\sigma^2(|\Lambda|^2 + N_\Phi) + P_\Phi^2\sigma^4]. \tag{61}$$

The integral in Equation 59 is a calculation of the overlap of the two probability distributions. A large overlap corresponds to a high probability of tracking loss, while a small overlap implies a low probability of tracking loss. Thus, using the Gaussian approximation above, we can say that tracking failure will occur when the difference in means is less than the sum of the $3\sigma_{Z(s)}$ points for the two distributions. This will be when

$$\overline{Z(s = s_\nu)} - \overline{Z(s \neq s_\nu)} = \beta\left[\sigma_{Z(s=s_\nu)} + \sigma_{Z(s\neq s_\nu)}\right] \tag{62}$$

where in most cases we shall set $\beta = 3$. If we combine Equations 60, 61, and 62 we find that the visibility at which tracking will fail is

$$V^2 = \frac{8\beta}{MN_\nu^2}\left(N_\nu + P_\nu\sigma^2 + \frac{1}{\beta}\sqrt{M(N_\nu^2 + P_\nu^2\sigma^4 + 2p_\nu\sigma^2N_\nu)}\right). \tag{63}$$

This equation can also be solved numerically for N_ν. This has been done for the various parameters sets shown in Figure 5, where small vertical lines have been plotted at the photon count rate predicted by Equation 63. This plot demonstrates that the Gaussian approximation works well, even for low values of M.

6. SAMPLE TIME AND APERTURE SIZE OPTIMIZATION

With the approximations for correlation measurement SNR set out in Section 4 and the Gaussian approximation given in the previous section for tracking failure, it is possible to

investigate optimum sample times and aperture sizes for the two measurements. In order to do this we require expressions for the temporal and spatial correlation transfer factors of the atmosphere. The temporal coherence transfer factor is given by (Buscher 1988)

$$\eta_{\mathrm{t}}^2 = \frac{2}{\tau}\int_0^{\tau}\left(1-\frac{t}{\tau}\right)\exp\left[-(\frac{t}{\tau_0})^{5/3}\right]dt, \tag{64}$$

and the spatial coherence transfer factor is given by (Tango & Twiss 1980)

$$\eta_{\mathrm{s}}^2 = \frac{\int T(\boldsymbol{\nu})B^2(\boldsymbol{\nu})\,d\boldsymbol{\nu}}{\int T(\boldsymbol{\nu})\,d\boldsymbol{\nu}}. \tag{65}$$

Once again $T(\boldsymbol{\nu})$ is the optical transfer function of the optical system, and the optical transfer function of the phase aberrations caused by the atmosphere is $B(\boldsymbol{\nu})$. Expressions for $T(\boldsymbol{\nu})$ and $B(\boldsymbol{\nu})$ can be found in the work by Fried (1966). This method for calculating the spatial coherence loss factor has been criticized by Buscher, who uses the results of a computer simulation instead. However, other simulations (ten Brummelaar et al. 1995) confirm Equation 65, and so we will use this expression in the calculations below. In either case, the general form of the coherence loss factor is the same, and the results will be very similar.

6.1. Correlation measurement

For correlation measurement we have, for all measurement schemes,

$$\mathrm{SNR}(V^2) \propto \begin{cases} \sqrt{M}\,N_\Phi\,V^2 & \text{for } \sigma = 0 \\ \sqrt{M}\,N_\Phi^2\,V^2 & \text{for } \sigma \neq 0. \end{cases} \tag{66}$$

Changing the sample time will affect all of the parameters in Equation 66. The visibility V will be proportional to the temporal coherence transfer factor given in Equation 64, the average number of photons arriving per sample time will be proportional to the sample time, while the number of samples M in a given integration time will be inversely proportional to the sample time. This results in

$$\mathrm{SNR}(V^2) \propto \begin{cases} \tau^{1/2}\,\eta_{\mathrm{t}}^2 & \text{for } \sigma = 0 \\ \tau^{3/2}\,\eta_{\mathrm{t}}^2 & \text{for } \sigma \neq 0. \end{cases} \tag{67}$$

Changing the aperture size R will have a similar effect, except the number of integrations will not change and the average number of photons will be proportional to the aperture radius squared, and so

$$\mathrm{SNR}(V^2) \propto \begin{cases} R^2\,\eta_{\mathrm{s}}^2 & \text{for } \sigma = 0 \\ R^4\,\eta_{\mathrm{s}}^2 & \text{for } \sigma \neq 0. \end{cases} \tag{68}$$

The top plot in Figure (6) shows the SNR in arbitrary units for the these four cases.

From the point of view of SNR a noiseless detector has an optimum sample time of $1.6\tau_0$ and an optimum aperture size of $2.5r_0$. Taking into account the different definitions of η_{s}, this is exactly the same as the results of Buscher. Once detector noise has been added, however, no local maximum occurs in the SNR curves and both the optimum aperture size and sample time go to infinity. This is similar to the non tilt corrected case discussed by Buscher. Obviously it is neither possible nor desirable to have extremely large sample times

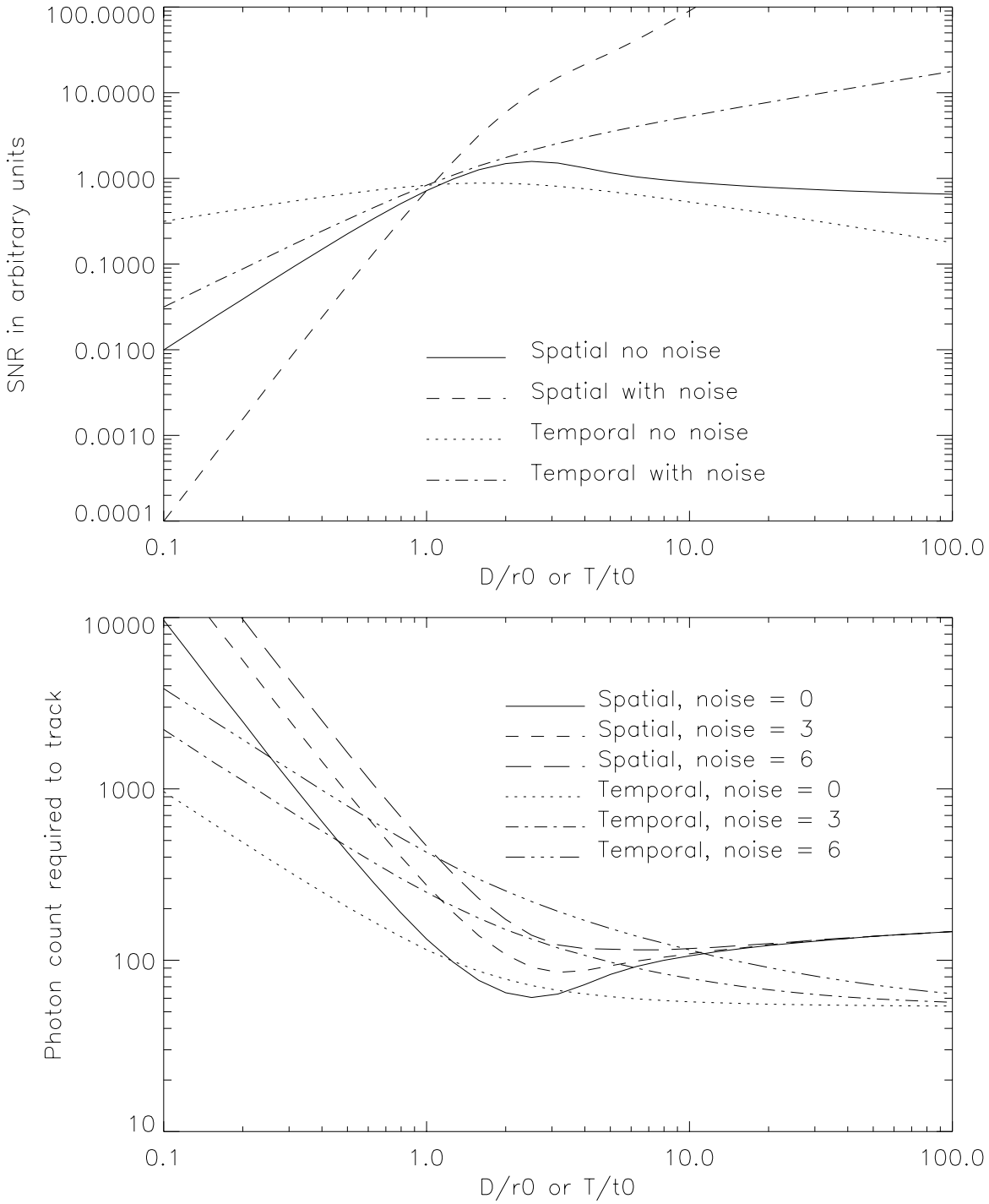

FIGURE 6. Above: The SNR of correlation measurement at low photon rates as a function of aperture size and sample time for a noiseless and a noisy detector. Below: The photon counts required in a single sample over each r_0 cell in a time period of τ_0 using a 32 pixel detector in order to track the fringe envelope as a function of aperture size and sample time for various noise levels.

or apertures which will produce very low measured visibilities, albeit with high SNR. As will be shown below, this is not the case for group delay tracking, and when using the same detection system to do both fringe tracking and correlation measurement it would be best to choose the aperture size that optimizes fringe tracking performance. Figure 6 also shows that the curves for the noisy detector change slope at approximately the same point at which the noiseless detector SNR is optimized. This indicates that while the SNR will increase beyond this point, the relative increase in SNR is reduced. Thus using the optimum sample time for a noiseless detector may be the best choice even if you are using a noisy detector.

6.2. Fringe tracking

Unfortunately, no simple approximations are available for group delay tracking, so no general case can be investigated. The lower plot in Figure 6 shows the count rates required per r_0 cell in a time period of τ_0 for group delay tracking using Equation 63 over 32 pixels with noise levels of $\sigma = 0$, $\sigma = 3$ and $\sigma = 6$ and no integration ($M = 1$). Once again, Equations 64 and 65 have been used for the visibility, and the counts have been scaled by R^2 for the spatial case and τ for the temporal case.

For a noiseless detector, the optimum aperture size is once again $2.5r_0$, the same as that for correlation measurement. As noise is added to the detector, this optimum aperture size increases to $3r_0$ for $\sigma = 3$ and $7r_0$ for $\sigma = 6$. With higher noise levels, no local minimum exists. This plot also shows that it is only at the smaller apertures that the noise affects tracking performance, reflecting the fact that for large aperture sizes the photon count overwhelms the detector noise. Thus the optimum aperture size for a noisy detector should be chosen based on fringe tracking rather than correlation measurement.

There is no clear optimum sample time for either the noiseless or noisy detector cases, although the longer the sample time the better the probability of fringe tracking. If too large a sample time is chosen, the fringe envelope can move significantly, smearing out the peak in the channeled spectrum and making fringe tracking impossible. The sample time should not be longer than 2-3 times τ_0. If longer times are needed for faint objects, longer integrations should be used. The paper by Lawson (1994) contains a discussion of these problems.

7. CONCLUSION

High DQE noiseless detectors such as an APD will always have the best performance for both fringe tracking and correlation measurement. Unfortunately, these devices are not available in arrays and they have a high per-pixel cost. This work has shown that when choosing a detector that will allow fringe tracking on the faintest possible object with the lowest possible visibility and shortest possible sample time, a noisy high-DQE detector like a bare CCD becomes an attractive alternative, especially if the flexibility of on-chip rebinning is taken into account. It has also been shown that these devices can be used for correlation measurement although they only match the performance of a lower DQE noiseless array detector rather than improve on it. In the case of group delay tracking an optimum aperture size exists for a noisy detector and a method for calculating this has been given. In the case of sample times and correlation measurement no clear optimums were found and the optimums for a noiseless detector ($2.5r_0$ for aperture size and $1.6\tau_0$ for sample time) should be used.

CCDs with a readout noise figure of $\sigma = 6$ are now available, and it is to be hoped that noise levels of $\sigma = 3$ will be achieved on a production basis soon. Based on these calculations, a small low-noise CCD has a high enough DQE to make up for its readout noise, making it a good detector for group delay tracking. Once in place it will also be possible to use this array detector for parallel correlation measurements in multiple spectral bands.

8. REFERENCES

Beletic, J.W. 1994, "Use of CCD Technology for Fringe Tracking in the CHARA Array," in *The CHARA Array: Final Report to the National Science Foundation,* (Report to NSF: Cooperative Agreement 90-08941, Atlanta), Appendix P

Beletic, J.W. & Goody, R.M. 1992, "Recovery of Planetry Images by Speckle Imaging," Applied Optics, **31**, No 32, 6909-6921

Beletic, J.W., Zadnick,J.A., Tritsch, C.L., & DuVarney, R.C. 1991, "Georgia Tech Low Light Level Imaging System, " in *SPIE Proc: High Resolution Imaging by Interferometry II,* J.M. Beckers & F. Merkle, ed., pp. 12

ten Brummelaar, T.A., Bagnuolo Jr., W.G., & Ridgway, S.T. 1995, "Strehl ratio and visibility in long-baseline stellar interferometry," Optics Letters, **20**, 521-523

Buscher, D. 1988, "Optimizing a ground-based optical interferometer for sensitivity at low light levels," MNRAS, **235**, 1203-1226

Davis, J. et al. 1994, "Progress in commissioning the Sydney University Stellar Interferometer (SUSI), " in Proc. SPIE conference on *Advanced Telescopes & Instrumentation,* **2200**, 231-241

Fried, D.L. 1966, "Optical resolution through a randomly inhomogeneous medium for very long and very short exposures," JOSA, **56**, 1372-1379

Kulkarni, S.R., Prasad, S., & Nakajima, T. 1991, "Noise in Optical Synthesis Images. II. Sensitivity of an ${}^nC_2$ Interferometer with Bispectrum Imaging," JOSA-A, **8**, 499-510

Lawson, P.R. 1993, "Artifacts in PAPA Camera Images," Applied Optics, **33,** 1146-1153

Lawson, P.R. 1994, "Group delay tracking in optical stellar interferometry using the Fast Fourier Transform," JOSA-A, **12**, 366-374

McAlister, H.A. et al. 1994, "The CHARA Array, " in Proc. SPIE conference on *Advanced Telescopes & Instrumentation,* **2200**, 129-139

Nightingale, N.S. 1991, "A New Silicon Avalanche Photodiode Photon Counting Detector for Astronomy," Experimental Astronomy, **1(6)**, 407-422

Papaliolios, C. & Mertz, L. 1982, "New two-dimensional photon camera," in *Instrumentation in Astronomy IV*, D.L. Crawford, ed, Proc. Soc. Photo-Opt, Instrum. Eng. **331**, 360-364

Roddier, F. 1986, "Pupil plane versus image plane in Michelson stellar interferometry," JOSA-A, **3**, 2160-2166

Shao, M. et al. 1988, "The Mark III stellar interferometer," A&A, **193**, 357-371

Tango, W.J. & Twiss, R.Q. 1980, "Michelson Stellar Interferometry," Progress in Optics, **XVII**, 239-277

Traub, W.A. 1990, "Constant-dispersion grism spectrometer for channeled spectra," JOSA-A, **7**, 1779-1791

Walkup, J.F. & Goodman, J.W. 1973, "Limitations of fringe-parameter estimation at low light levels," JOSA, **63**, 399-407